Theoretical analysis of tensile stresses and displacement in orthotropic circular column under diametrical compression

Takashi Tsutsumi[*1], Hiroshi Iwashita[2a] and Kagenobu Miyahara[1b]

[1]*Department of Civil Engineering, Kagoshima National College of Technology, Kirishima, Kagoshima, 899-5193, Japan*
[2]*Kyushu Railway Company, Fukuoka, 812-8566, Japan*

Abstract. This paper shows the solution for an orthotropic disk under the plane strain condition obtained with complex stress functions. These stress functions were induced by Lekhnitskii and expanded by one of the authors. Regarding diametrical compression test, the finite element method poses difficulties in representing the concentrated force because the specimens must be divided into finite elements during calculation. On the other hand, the method shown in this study can exactly represent this force. Some numerical results are shown and compared with those obtained under the plane stress condition for both stress and displacement. This comparison shows that the differences between the tensile stresses occurred under the plane strain condition and also that the differences under a plane stress condition increase as the orthotropy ratio increases for some cases.

Keywords: orthotropy; diametrical compression; tensile stress; displacement; plane strain condition.

1. Introduction

   The diametrical compression test is a simple and relatively inexpensive test for measuring the tensile strength of brittle material. This test is performed by placing a disk or circular column between two (rigid) plates and applying a diametrical compressive load. The test induces a biaxial stress state in which the stress at the center of the disk is compressive in the x-direction (σ_x), and tensile in the y-direction (σ_y). Theoretically, for an isotropic material, the tensile stress reaches a maximum at the constant magnitude of $P/(\pi R)$, where P is the applied load and R is the radius of the disk (Sokolnikoff 1956, Timoshenko 1970). Because tensile strength is smaller than compressive strength for many brittle materials, the material undergoes tensile failure first. Recently, this test, known as the Brazilian test in rock mechanics, was described in some works covering isotropic material alone (Lavrov and Vervoort 2002, Markides *et al.* 2010). However, some materials for this test exhibit orthotropicity as seen in experimental work for specimens containing some layers

*Corresponding author, Associate Professor, E-mail: tsutsumi@kagoshima-ct.ac.jp
[a]Assistant Manager
[b]Student of Advanced Course

(Tavallali and Vervoort 2010) or numerical simulation (Cai and Kaiser 2004). Stresses and strains were obtained by Jianhong *et al.* (2009) for the case in which the elastic modulus in tension is different from that in compression.

The circular plane problems concerning homogeneous material under diametrical compression were addressed in some studies. Cauweleart and Eckmann (1994) obtained a solution using the theoretical results for a semi-infinite plate under concentrated force. Lemmon *et al.* (Lemmon and Blackketter 1996) evaluated stresses and displacements using the finite element method (FEM) in which the applied load areas are very narrow. Lekhnitskii (1968) attempted to obtain a solution using a complex power series, but was unable to obtain the stress field completely because of the lack of equations for first term of the boundary conditions. Chen *et al.* (1998), Exadaktylos and Kaklis (2001), Exadaktylos (2001) and Claesson and Bohloli (2002) used Lekhnitskii's solution for rock specimens. They obtained the first term of the solution by direct indication under the boundary condition. Therefore, the method of determining complex coefficients in the first term was not shown in their work. One of the authors (Kawakubo *et al.* 1996) shows a method of completely determining the complex coefficients in the first term of Leknitskii's solution which included the condition that rigid rotation does not occur in the specimen. Good agreement between the numerical results obtained using this solution and those obtained by FEM was found for loading width equal to 2, 4, and 8% of circumference (Tsutsumi and Hirashima 2000).

In this paper, the solution to the plane strain problem is obtained using Lekhnitskii's solution based on the condition that rigid body rotation does not occur in the specimen. This solution is valid for the column-shaped specimens which were subjected to a diametrical compression test. Specimens described in this paper are orthotropic but are also homogeneous and comprise a continuum without layers or micro-cracks. Furthermore, the numerical results for stress and displacement are shown and compared with the results obtained under the plane stress condition.

2. Fundamental equations

In this paper, the problem of the application of opposing concentrated loads P to the diametrical axis of an orthotropic column specimen of radius a is treated as shown in Fig. 1; Here, φ is the angle between the loading axis and the principal elastic axis, and E_1 and E_2 are the respective elastic moduli in the direction of the principal elastic axis.

By denoting the loading axis as x, and the perpendicular direction in the plane of the loading axis as y, the following equations representing the resultant forces on surface X_n and Y_n, going anticlockwise from the x-axis in the x and y directions, on the boundary circumference of a column-shaped specimen, which are related to stress components σ_x, σ_y and t_{xy} are obtained
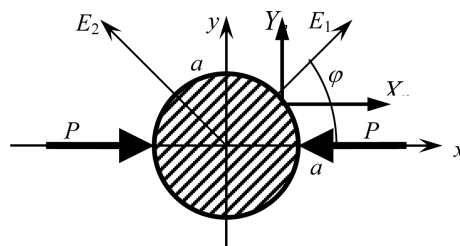

Fig. 1 Orthotropic circular disk under diametrical compression

$$X_n = \sigma_x \cos(n,x) + \tau_{xy} \cos(n,y)$$
$$Y_n = \tau_{xy} \cos(n,x) + \sigma_y \cos(n,y) \tag{1}$$

The stress components σ_x, σ_y and τ_{xy}, and the displacement components u_x and u_y are expressed by the following (Lekhnitskii 1968).

$$\sigma_x = 2\mathrm{Re}[\mu_1^2 \Phi_1'(z_1) + \mu_2^2 \Phi_2'(z_2)]$$

$$\sigma_y = 2\mathrm{Re}[\Phi_1'(z_1) + \Phi_2'(z_2)]$$

$$\tau_{xy} = -2\mathrm{Re}[\mu_1 \Phi_1'(z_1) + \mu_2 \Phi_2'(z_2)] \tag{2}$$

$$u_x = 2\mathrm{Re}[p_1 \Phi_1(z_1) + p_2 \Phi_2(z_2)]$$
$$u_y = 2\mathrm{Re}[q_1 \Phi_1(z_1) + q_2 \Phi_2(z_2)] \tag{3}$$

Here, Re denotes the real part of the complex functions in brackets. $\Phi_k'(z_k)$ means the first derivative of $\Phi_k(z_k)$ with respect to z_k. By using a_{ij}' $(i,j = 1, 2, 3, 6)$ for the elastic compliance values of the specimens with a sufficient depth under the plane strain condition, as shown in Fig. 2(a), the following relations are obtained

$$\varepsilon_x = a_{11}' \sigma_x + a_{12}' \sigma_y + a_{13}' \sigma_z$$

$$\varepsilon_y = a_{12}' \sigma_x + a_{22}' \sigma_y + a_{23}' \sigma_z$$

$$\varepsilon_z = a_{13}' \sigma_x + a_{23}' \sigma_y + a_{33}' \sigma_z$$

$$\gamma_{xy} = a_{66}' \tau_{xy}, \; \gamma_{yz} = \gamma_{zx} = 0 \tag{4}$$

Here, ε and γ respectively denote the vertical strain and shear strain in the direction indicated by subscripts. The complex parameters μ_1, μ_2 in Eq. (2) are obtained as complex roots of the following equation

$$a_{11}' \mu^4 - 2a_{16}' \mu^3 + (2a_{21}' + a_{66}')\mu^2 - 2a_{26}' \mu + a_{22}' = 0 \tag{5}$$

Under the plane stress condition without sufficient depth, as shown in Fig. 2(b), and when the direction of E_1 coincides with the coordinate axis ($\varphi = 0$), the elastic compliance values are expressed as follows

$$a_{11}^0 = (1 - \nu_{13}\nu_{31})/E_1, \quad a_{22}^0 = (1 - \nu_{23}\nu_{32})/E_2$$
$$a_{12}^0 = -(\nu_{12} + \nu_{23}\nu_{32})/E_1, \; a_{66}^0 = 1/G, \; a_{16}^0 = a_{26}^0 = 0 \tag{6}$$

a_{33}^0 is the elastic modulus for the depth direction. When the direction of E_1 is not coincident with the coordinate axis, having an arbitrary angle of φ, the elastic compliance values a_{ij} $(i, j = 1, 2, 3, 6)$ under the plane stress condition are expressed by the following.
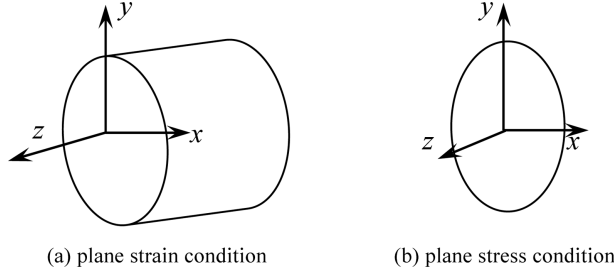
<center>(a) plane strain condition   (b) plane stress condition</center>

<center>Fig. 2 Plane strain condition and plane stress condition</center>

$$a_{11} = a_{11}^0\cos^4\varphi + (2a_{12}^0 + a_{66}^0)\sin^2\varphi\cos^2\varphi + a_{22}^0\sin^4\varphi + (a_{16}^0\cos^2\varphi + a_{26}^0\sin^2\varphi)\sin 2\varphi$$

$$a_{22} = a_{11}^0\sin^4\varphi + (2a_{12}^0 + a_{66}^0)\sin^2\varphi\cos^2\varphi + a_{22}^0\cos^4\varphi - (a_{16}^0\sin^2\varphi + a_{26}^0\cos^2\varphi)\sin 2\varphi$$

$$a_{12} = a_{12}^0 + (a_{11}^0 + a_{22}^0 - 2a_{12}^0 - a_{66}^0)\sin^2\varphi\cos^2\varphi + \frac{1}{2}(a_{26}^0 - a_{16}^0)\sin 2\varphi\cos 2\varphi$$

$$a_{66} = a_{66}^0 + 4(a_{11}^0 + a_{22}^0 - 2a_{12}^0 - a_{66}^0)\sin^2\varphi\cos^2\varphi + 2(a_{26}^0 - a_{16}^0)\sin 2\varphi\cos 2\varphi$$

$$a_{16} = \left[a_{22}^0\sin^2\varphi - a_{11}^0\cos^2\varphi + \frac{1}{2}(2a_{12}^0 + a_{66}^0)\cos 2\varphi\right]\sin 2\varphi$$

$$+ a_{16}^0\cos^2\varphi(\cos^2\varphi - 3\sin^2\varphi) + a_{26}^0\sin^2\varphi(3\cos^2\varphi - \sin^2\varphi)$$

$$a_{26} = \left[a_{22}^0\cos^2\varphi - a_{11}^0\sin^2\varphi - \frac{1}{2}(2a_{12}^0 + a_{66}^0)\cos 2\varphi\right]\sin 2\varphi$$

$$+ a_{16}^0\sin^2\varphi(3\cos^2\varphi - \sin^2\varphi) + a_{26}^0\cos^2\varphi(\cos^2\varphi - 3\sin^2\varphi) \tag{7}$$

In addition, using these equations the elastic compliance a'_{ij} under the plane strain condition in Eq. (4) is obtained from the following relations

$$a'_{ij} = a_{ij} - \frac{a_{i3}a_{j3}}{a_{33}^0} \quad (i,j = 1,2,6), \quad a'_{33} = 0 \tag{8}$$

Because column specimens are treated as having depth in the z-direction in the present paper, a model is made under the plane strain condition.

3. Formulation of the problem

Next, a problem is formulated, in which a concentrated load P is applied diametrically to an orthotropic column. The resultant forces for the x-directions and y-directions on the surface are expanded as Fourier series with M terms, as follows

$$\int_0^s X_n ds = \beta_0 + \sum_{m=1}^{M}(\beta_m e^{im\theta} + \bar{\beta}_m e^{-im\theta})$$

$$-\int_0^s Y_n ds = \alpha_0 + \sum_{m=1}^{M}(\alpha_m e^{im\theta} + \bar{\alpha}_m e^{-im\theta}) \tag{9}$$
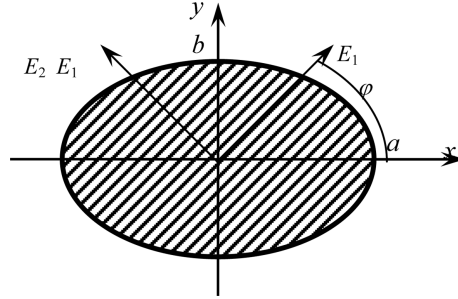
Fig. 3 Elliptic disk represented by the solution in this study

Here, the bar denotes the complex conjugate. When the concentrated load P is applied to the x-axis, α_m and β_m are expressed as follows

$$\alpha_m = 0, \quad \beta_m = -\frac{iP}{2m\pi}\{1-(-1)^m\} \tag{10}$$

The complex stress functions for an orthotropic elliptic plate with the major axis a and the minor axis b, as shown in Fig. 3, are expanded as the series expressed below (Lekhnitskii 1968)

$$\Phi_1(z_1) = A_0 + A_1 z_1 + \sum_{m=2}^{M} A_m P_{1m}(z_1)$$

$$\Phi_2(z_2) = B_0 + B_1 z_2 + \sum_{m=2}^{M} B_m P_{2m}(z_2) \tag{11}$$

Here $P_{km}(z_k)$ ($k = 1, 2$) is a power series of the m-th order and is expressed by the following equation.

$$P_{km}(z_k) = -\frac{1}{(a-i\mu_k b)^m}\left\{\left(z_k+\sqrt{z_k^2-a^2-\mu_k^2 b^2}\right)^2 + \left(z_k-\sqrt{z_k^2-a^2-\mu_k^2 b^2}\right)^2\right\} \quad (k=1,2) \tag{12}$$

In the present problem, because the circular column-shaped specimens are used, it can be assumed that $a = b$ for the purpose of calculation. The complex variable z_k and power series $P_{km}(z_k)$ are represented on the cylindrical boundary as follows

$$z_k = \frac{1}{2}\{(a-\mu_k b)e^{i\theta} + (a+i\mu_k b)e^{-i\theta}\}$$

$$P_{km} = -(e^{im\theta}+t_k^m e^{-im\theta}), \quad t_k = \frac{a+i\mu_k b}{a-i\mu_k b} \quad (k=1,2) \tag{13}$$

By using the complex functions $\Phi_k(z_k)$, the resultant stresses are expressed as follows

$$\int_0^s X_n ds = \mathrm{Re}[\mu_1\Phi_1(z_1)+\mu_2\Phi_2(z_2)]$$

$$-\int_0^s Y_n ds = \mathrm{Re}[\Phi_1(z_1)+\Phi_2(z_2)] \tag{14}$$

By substituting Eq. (13) into Eq. (11), and obtained equations into Eq. (14), the equations for assigning the resultant stress on the boundary are obtained. Furthermore, the coefficients of the

corresponding terms of $e^{im\theta}$ and $e^{-im\theta}$ $(1 \leq m \leq M)$ are compared with each other, resulting in the following equations

$$A_1 + B_1 + \overline{A}_1 + \overline{B}_1 = \frac{1}{a}(\alpha_1 + \overline{\alpha}_1)$$

$$\mu_1 A_1 + \mu_2 B_1 + \overline{\mu}_1 \overline{A}_1 + \overline{\mu}_2 \overline{B}_1 = \frac{1}{ib}(\overline{\alpha}_1 - \alpha_1) = \frac{1}{a}(\beta_1 + \overline{\beta}_1)$$

$$\mu_1^2 A_1 + \mu_2^2 B_1 + \overline{\mu}_1^2 \overline{A}_1 + \overline{\mu}_2^2 \overline{B}_1 = \frac{1}{ib}(\overline{\beta}_1 - \beta_1)$$

$$(m = 1) \tag{15}$$

$$A_m + B_m + \overline{t}_1^m \overline{A}_m + \overline{t}_2^m \overline{B}_m = -\alpha_m$$

$$\mu_1 A_m + \mu_2 B_m + \overline{\mu}_1 \overline{t}_1^m \overline{A}_m + \overline{\mu}_2 \overline{t}_2^m \overline{B}_m = -\beta_m$$

$$t_1^m A_m + t_2^m B_m + \overline{A}_m + \overline{B}_m = -\overline{\alpha}_m$$

$$\mu_1 t_1^m A_m + \mu_2 t_2^m B_m + \overline{\mu}_1 \overline{A}_m + \overline{\mu}_2 \overline{B}_m = -\overline{\beta}_m$$

$$(m \geq 1) \tag{16}$$

For the case of $m = 1$, there are only three equations for the four unknown quantities of the real and imaginary parts of A_1 and B_1, respectively, so these equations are unsolved. For this reason, the condition that the rigid body rotation is zero is additionally introduced, resulting in the following equation (Kawakubo *et al.* 1996)

$$(q_1 - \mu_1 p_1)A_1 + (q_2 - \mu_2 p_2)B_1 + (\overline{q}_1 - \overline{\mu}_1 \overline{p}_1)\overline{A}_1 + (\overline{q}_2 - \overline{\mu}_2 \overline{p}_2)\overline{B}_1 = 0 \tag{17}$$

where

$$p_1 = a'_{11}\mu_1^2 + a'_{12}, \ \ p_2 = a'_{11}\mu_2^2 + a'_{12}$$

$$q_1 = (a'_{12}\mu_1^2 + a'_{22})/\mu_1, \ \ q_2 = (a'_{12}\mu_2^2 + a'_{22})/\mu_2 \tag{18}$$

By adding Eq. (17) to Eq. (15), A_1 and B_1 can be obtained completely.

4. Results and discussion

4.1 Stress analysis

Fig. 4 shows that the distribution of the tensile stress occurring on the loading radius. The tensile stress in these figures is normalized by the tensile stress $P/(\pi a)$ that occurs uniformly on the loading radius when the specimen is isotropy. Here, the angle of the direction of the Young's modulus E_1 in the loading direction φ was set to 0°, 15°, 30°, 45°, 60°, 75° and 90°. (a) shows the results for near-isotropic case, (b) for $E_2/E_1 = 2.0$ and (c) for $E_2/E_1 = 5.0$. The elastic modulus for the depth direction

(a) Near-isotropy (E_2/E_1=0.98)
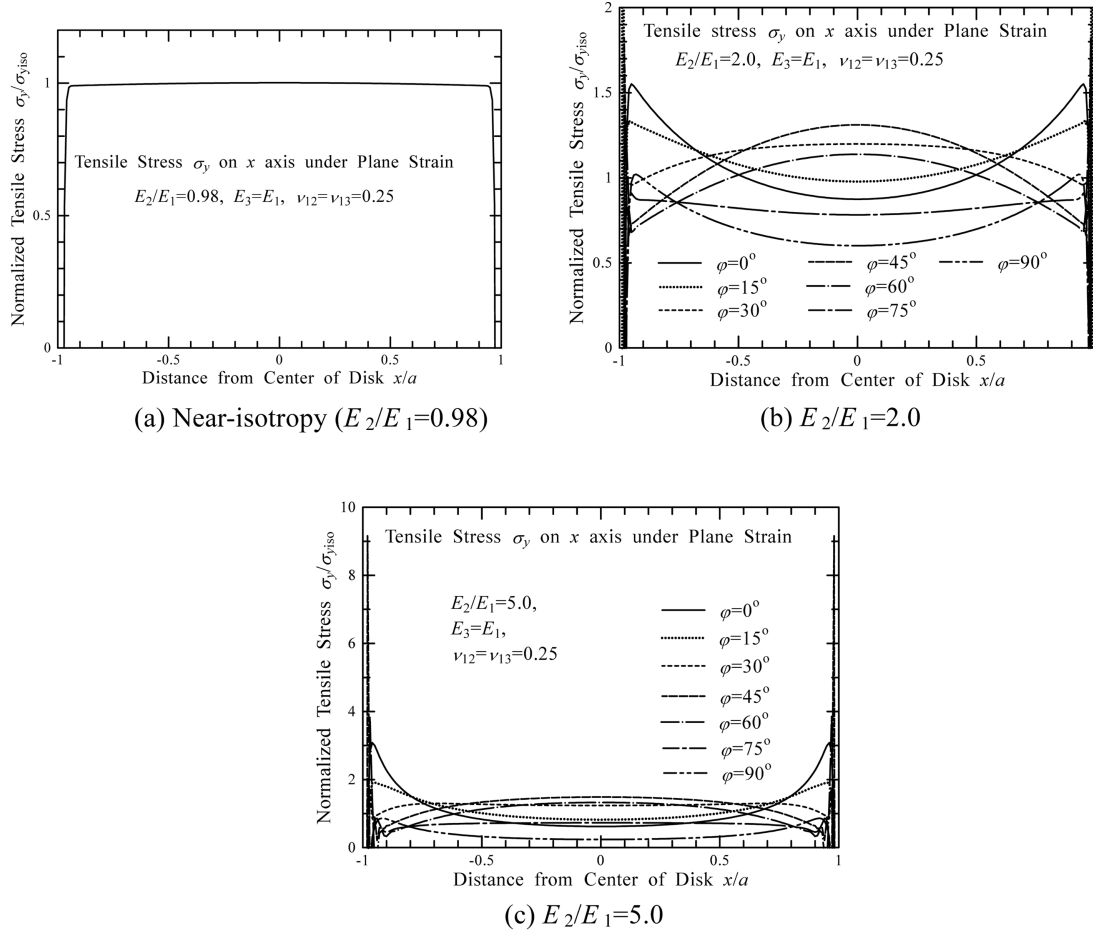

(b) E_2/E_1=2.0

(c) E_2/E_1=5.0

Fig. 4 Distribution of tensile stress for various directions of elastic axis

was set equal to E_1 for both cases. The author's method is not valid for $E_2/E_1 = 1.0$, so $E_2/E_1 = 0.98$ is chosen for the near-isotropic case.

In an analysis using a series as in the present study, the convergence and the accuracy of the calculated value must be always discussed. The number of terms M in Eq. (11) affects the calculated values. A large number of terms is necessary for problems involving concentrated force, because the resultant forces are represented as step functions. A_n and B_n converge to zero with two hundred and fifty terms. The error is 6% with one hundred terms, 3% with one hundred fifty terms and 1% with two hundred terms. In this paper, calculations were carried out with two hundred fifty terms.

In each case, the distribution of the tensile stress on the loading radius is symmetrical. It can be observed that the uniform tensile stress occurs along the loading axis except at the loading points under the near-isotropic condition. For $\varphi = 0°$, $15°$, $75°$, and $90°$, the maximum is found at $|x/a| > 0.9$, and the minimum at the center of the specimen. For the case of $\varphi = 30°$ and $\varphi = 60°$, the maximum is found in a very narrow range around $x/a = 0.98$, as is the case with the analysis for the plane stress condition. In the analysis for the plane stress condition, the maximum was found at this
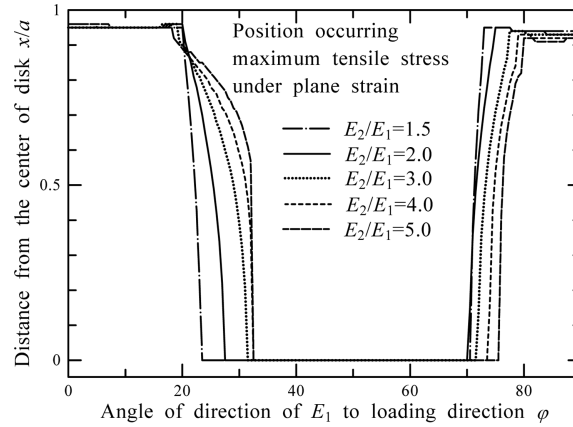
Fig. 5 Relation between the angle φ and distance at which maximum tensile stress occurs

position from the analysis based on the theoretical solution for loading widths of 8, 4 and 2 % of the circumference, same as results from the finite element analysis. Taking account of this fact, these phenomena, particularly when observed during concentrated loading, are considered as noise due to the Gibbs phenomenon caused by Fourier series expansion of the stepwise loading. Consequently it is reasonable to regard the local maximum found at the center of the specimen as maximum. The maximum values of the tensile stress for $\varphi = 0°$, 45°, and 90° are respectively 1.55, 1.31 and 1.02 times larger than those of the isotropic case for $E_2/E_1 = 2.0$, and 3.08, 1.49 and 0.86 times larger than those for $E_2/E_1 = 5.0$. For $\varphi = 0°$, namely for the application of load in the direction of small elastic modulus, the maximum values of the tensile stress for $E_2/E_1 = 5.0$ are larger than those for $E_2/E_1 = 2.0$. For $\varphi = 45°$, the maximum values for $E_2/E_1 = 5.0$ are still larger than those for $E_2/E_1 = 2.0$, but the difference is smaller in comparison with the case of $\varphi = 0°$. In contrast, for the case of $\varphi = 90°$, in which the loading is made to the direction of large elastic modulus, the maximum values of the tensile stress for $E_2/E_1 = 5.0$ are smaller than those for $E_2/E_1 = 2.0$.

Fig. 5 shows the relation between the angle of the direction of E_1 to the loading direction φ and the distance between the center of the specimen and the point where the maximum tensile stress on the loading radius occurs. The orthotropy ratio E_2/E_1 was set to 1.5, 2.0, 3.0, 4.0 and 5.0. Also, the distance is normalized by radius a of the specimen. For all orthotropy ratios, the maximum tensile stress occurs near the loading point when the angle between the direction of E_1 or E_2 and loading direction is small. Furthermore, the maximum tensile stress occurs at the center of the specimen between $\varphi = 23.5°$ and $\varphi = 70.5°$ for $E_2/E_1 = 1.5$, 27.5° and 70.0° for 2.0, 31.5° and 71.5° for 3.0, 32.5° and 73.5° for 4.0, and 32.5° and 75.5° for 5.0, respectively.

Fig. 6 shows a comparison of the distribution of the tensile stress on the loading radius under the plane strain condition with that under the plane stress condition for $\varphi = 0°$, 45° and 90°. The tensile stress is normalized by the tensile stress $P/(\pi a)$ which occurs uniformly on the loading radius when the specimen is isotropy (Tsutsumi and Hirashima 2000). (a) shows the results for $E_2/E_1 = 2.0$ and (b) for $E_2/E_1 = 5.0$, where the solid lines represent the plane strain condition and the dotted lines the plane stress condition. For $\varphi = 0°$ and $\varphi = 90°$ under the plane strain condition, as well as under the plane stress condition, the maximum is found at around $x/a = 0.95$ and the minimum at the center of the specimen. For $\varphi = 45°$, the maximum is found at the center of specimen. For $\varphi = 0°$, the

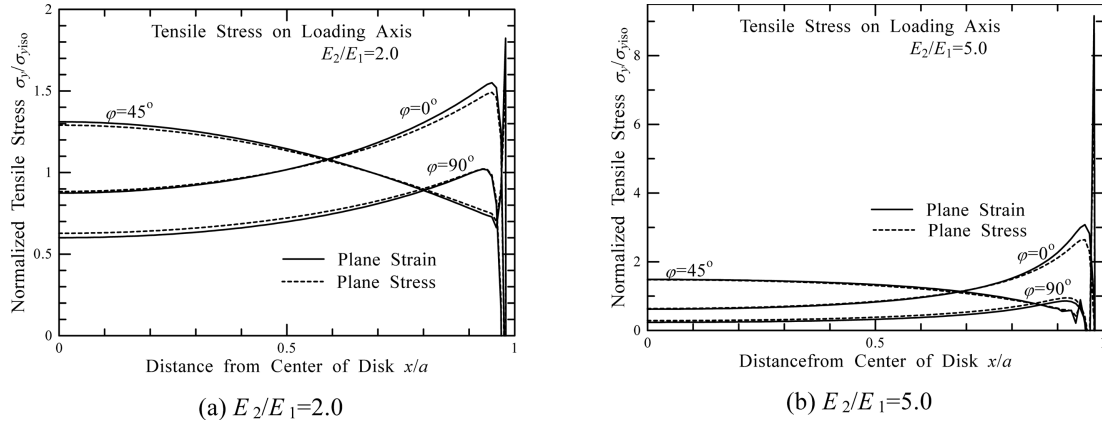(a) E_2/E_1=2.0   (b) E_2/E_1=5.0

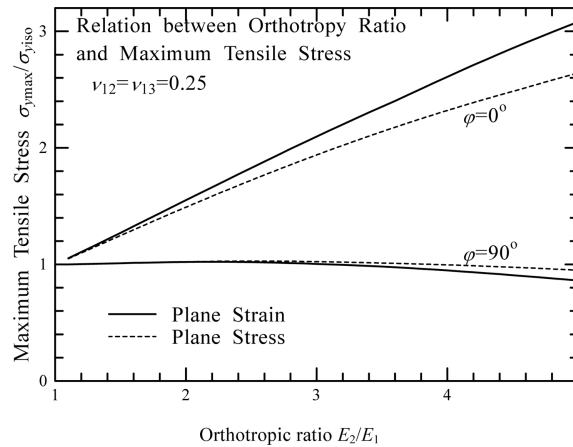Fig. 6 Distribution of tensile stress under plane stress and plane strain conditions

Fig. 7 Relation between orthotropy ratio and maximum tensile stress

maximum value of the tensile stress under the plane strain condition is larger than that under the plane stress condition. For $\varphi = 45°$, the maximum value under the plane strain condition is only slightly larger than that under the plane stress condition. In contrast, for $\varphi = 90°$ the maximum value of the tensile stress under the plane stress condition is larger than that under the plane strain condition. It addition, the difference between the maximum values under the two conditions is larger in the case of $E_2/E_1 = 5.0$ than in the case of $E_2 / E_1 = 2.0$.

Fig. 7 shows the relation between the orthotropy ratio and the maximum tensile stress for $\varphi = 0°$ and $\varphi = 90°$ under the plane stress condition, normalized by the tensile stress $P/(\pi a)$ which occurred in the isotropic case. The solid lines denote the plane strain condition and the dotted lines the plane stress condition. For $\varphi = 0°$, i.e., when the concentrated load is applied to the direction of smaller elastic modulus, the maximum values of the tensile stress increase with the increase of the isotropic ratio for the both conditions. The maximum tensile stress under the plane strain condition is larger than that under the plane stress condition, and the difference increases with increasing the orthotropy ratio. For $E_2/E_1 = 5.0$, under the plane stress condition, a maximum tensile stress of about

2.6 times larger than that of the isotropic case is found, while under the plane strain condition a maximum tensile stress of about 3.1 times larger is found. For $\varphi = 90^{\circ}$, i.e., when the concentrated load is applied in the direction of large elastic modulus, the maximum tensile stress increases slightly up to the orthotropy ratio of 2.5 under the plane stress condition, and up to the orthotropy ratio of 2.2 under the plane strain condition. Above these orthotropy ratios, the respective maximum tensile stresses start to decrease. In contrast to the case of $\varphi = 0^{\circ}$, the maximum tensile stress under the plane strain condition is smaller than that under the plane stress condition. For $E_2/E_1 = 5.0$, a similar maximum value of which magnitude is similar as that of the isotropic case is obtained under the plane stress condition, while the maximum value under the plane strain condition is 0.86 of that of the isotropic case under the plane strain condition.

4.2 Displacement analysis

The authors' method also enables displacement analysis to be performed for orthotropic material, because the complex coefficients in Eq. (11) can be determined completely.

Fig. 8 shows the deformation of the surface under diametrical compression in the case of $E_2/E_1 = 5.0$. The value of displacement in each figure is multiplied by $0.05E_1a/P$ to draw these displacements in this figure. Here, the angle of the direction of E_1 with respect to the loading axis φ was set to 0°, 30°, 60° and 90°. (a) shows the deformations under the plane strain condition and (b) under the plane stress condition. It can be observed that the deformation under the plane strain condition is nearly the same as that under the plane stress condition for all angles. For $\varphi = 0^{\circ}$ and 90°, namely when the loading direction is the same as the direction of principal material axis, the deformation is occurred in the loading direction at the loading points. Also, the displacement for $\varphi = 0^{\circ}$ is larger than that for $\varphi = 90^{\circ}$ because the Young's modulus along the loading direction for $\varphi = 0^{\circ}$ is smaller than that for $\varphi = 90^{\circ}$. For $\varphi = 30^{\circ}$, the deformation tends to occur in the direction of decreasing the Young's modulus though the displacement in the loading direction is the same as that for $\varphi = 0^{\circ}$. For $\varphi = 60^{\circ}$, the displacement in the loading direction is smaller than that for $\varphi = 30^{\circ}$, though the displacement perpendicular to the loading direction is smaller than that for $\varphi = 30^{\circ}$ at the loading point.

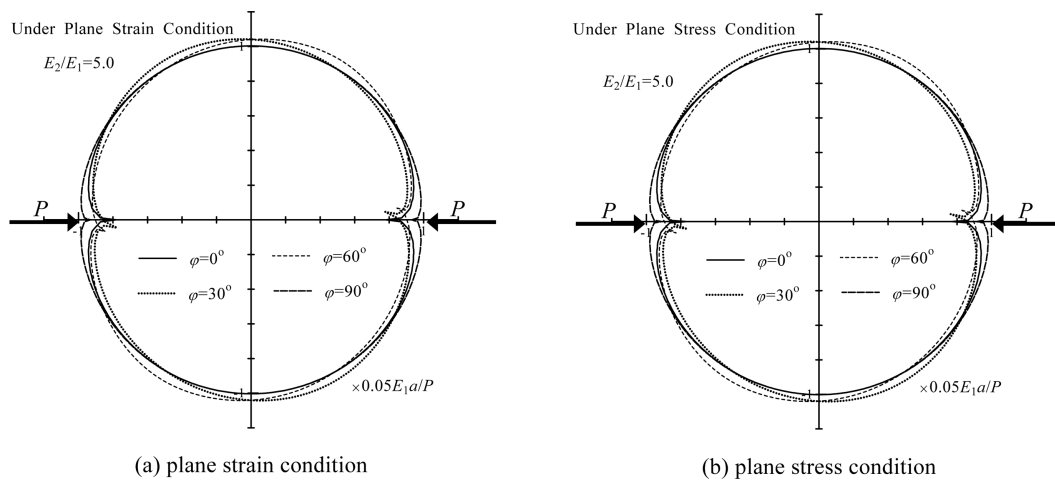(a) plane strain condition   (b) plane stress condition

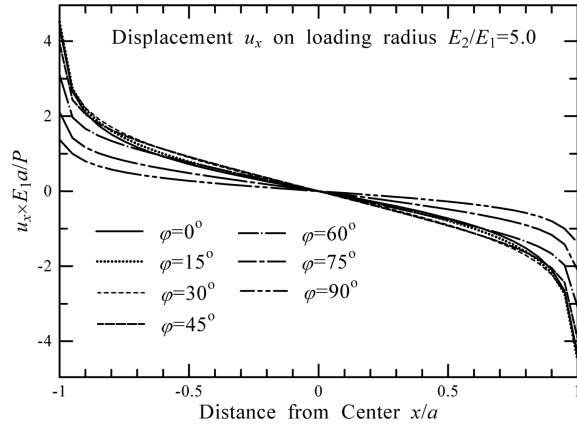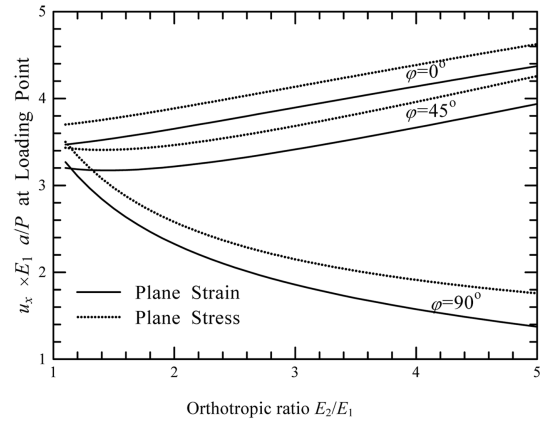Fig. 8 Deformation of circular specimen under diametrical compression

Fig. 9 Displacement u_x along loading radius

Fig. 10 Relation between orthotropy ratio and displacement at loaded point

Fig. 9 shows the displacement u_x on the loading radius for $E_2/E_1 = 5.0$. The displacement is multiplied by $E_1 a/P$ to make it the dimensionless value. Here, the angle of the direction of E_1 with respect to the loading axis φ was set to 0°, 15°, 30°, 45°, 60°, 75° and 90°. For all angles, the maximum displacement appears at the loading point. The displacement decreases as the distance from the loading point increases, and the displacement is zero at the center of the specimen. Furthermore, the distribution of the displacement on the loading radius is symmetrical for all angles. In this figure, the maximum displacement appears for $\varphi = 15°$ at the loading point. The second largest displacement appears for $\varphi = 30°$, and the third largest displacement for $\varphi = 0°$. The differences between these displacements are very small. Above $\varphi = 30°$, the displacement at the loading point decreases as the angle φ increases.

Fig. 10 shows the relation between the orthotropy ratio and the displacement in the loading direction at the loading point. The displacement is multiplied by $E_1 a/P$ to make it the dimensionless value. The solid lines denote the plane strain condition and the dotted lines the plane stress condition. Here, the angle of the direction of E_1 with respect to the loading direction φ was set to 0°, 45° and 90°. For all cases, the displacement under the plane strain condition is larger than that under the plane stress condition. For $\varphi = 0°$, the displacement increases as the orthotropy ratio increases. In this case, the Young's modulus perpendicular to the loading direction increases as the orthotropy ratio increases. For $\varphi = 45°$, which is the intermediate value between 0° and 90°, the displacement also increases as the orthotropy ratio increases. For $\varphi = 90°$, on the other hand, the displacement decreases as the orthotropy ratio increases because the Young's modulus in the loading direction increases as the orthotropy ratio increases. For all angles, the displacement under the plane strain condition is larger than that under the plane stress condition. However, it can be observed that the difference between the displacement under the plane strain condition and that under the plane stress condition is almost constant for $\varphi = 0°$ and 45°, and increases slightly for $\varphi = 90°$ as the orthotropy ratio increases.

Fig. 11 shows the relation between the angle of the direction of the Young's modulus E_1 with respect to the loading direction and the displacement in the loading direction at the loading point. The value of the displacement is multiplied by $E_1 a/P$ to make it the dimensionless quantity. The solid lines denote the plane strain condition and the dotted lines the plane stress condition. Here, the orthotropy ratio E_2/E_1 was set to 2.0, 3.0, 4.0 and 5.0. For all orthotropy ratios, the displacement
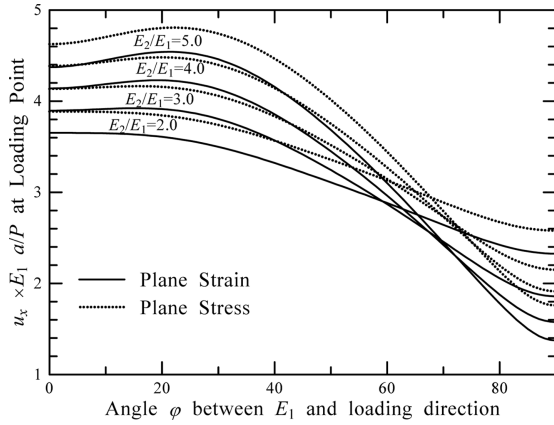
Fig. 11 Relation between orthotropic direction and displacement at loading point
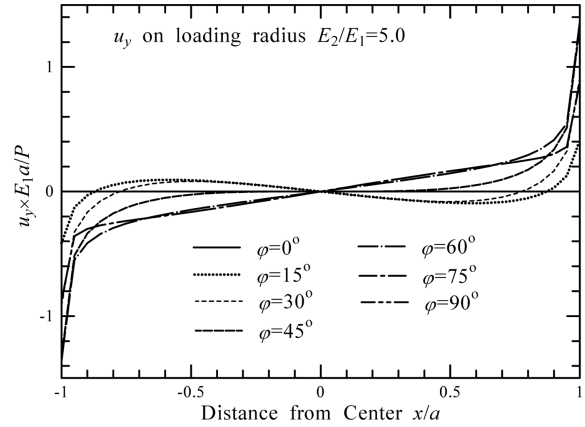

Fig. 12 Distribution of displacement perpendicular to loading direction

under the plane strain condition is smaller than that under the plane stress condition. For E_2/E_1=2.0, the maximum displacement appears at $\varphi = 0^o$ and the displacement decreases as angle φ increases under both conditions. The displacement at $\varphi = 0^o$ increases, though that at $\varphi = 90^o$ decreases as the orthotropy ratio increases. The maximum displacement that appears at φ is around 20° except when $E_2/E_1 = 2.0$. Also, the difference between the maximum displacement and the displacement at $\varphi = 0^o$ increases as the orthotropy ratio increases. For all orthotropy ratios, the displacement under the plane strain condition is larger than that under the plane stress condition. However, it can be observed that the difference between the displacement under the plane strain condition and that under the plane stress condition is almost constant though the angle φ increases for all orthotropy ratios.

Fig. 12 shows the distribution of the displacement perpendicular to the loading radius on the loading radius. The value of the displacement is multiplied by E_1a/P to make it the dimensionless value. Here, the angle of the Young's modulus E_1 with respect to the loading axis φ was set to 0°, 15°, 30°, 45°, 60°, 75° and 90°. For $\varphi = 0^o$ and 90°, i.e., when the loading axis is in the same direction as the principal elastic axis, the displacement does not appear. For other angles, the maximum displacement appears at the loading point, and the displacement disappears at the center of specimen. Furthermore, the displacement at the loading point tends to occur in the direction of decreasing the Young's modulus. However, it can be observed that the displacement in the direction of decreasing the Young's modulus appears inside the specimen for $\varphi = 15^o$ and 30°.

4.3 Relation between deformation and tensile stress on loading axis

Fig. 13 shows the relation between the tensile stress occurring on the loading axis and the deformation of the surface. (a), (b), (c) and (d) show $\varphi = 0^o$, 30°, 60° and 90° respectively. The orthotropy ratio was set to $E_2/E_1 = 5.0$. The solid lines denote the deformation of the surface, the broken lines the tensile stress on the loading radius, and the dotted lines the initial shape of the surface. The tensile stress is normalized by $5P/(\pi a)$ to make it the dimensionless value, and the value of displacement is also multiplied by $0.05E_1a/P$ to draw it in these figures.

For $\varphi = 0^o$ and 90°, i.e., the direction in which the principal elastic axis is same as that in the loading direction, the deformation appears in the loading direction at the loading point, and the

(a) $\varphi = 0°$

(b) $\varphi = 30°$

(c) $\varphi = 60°$
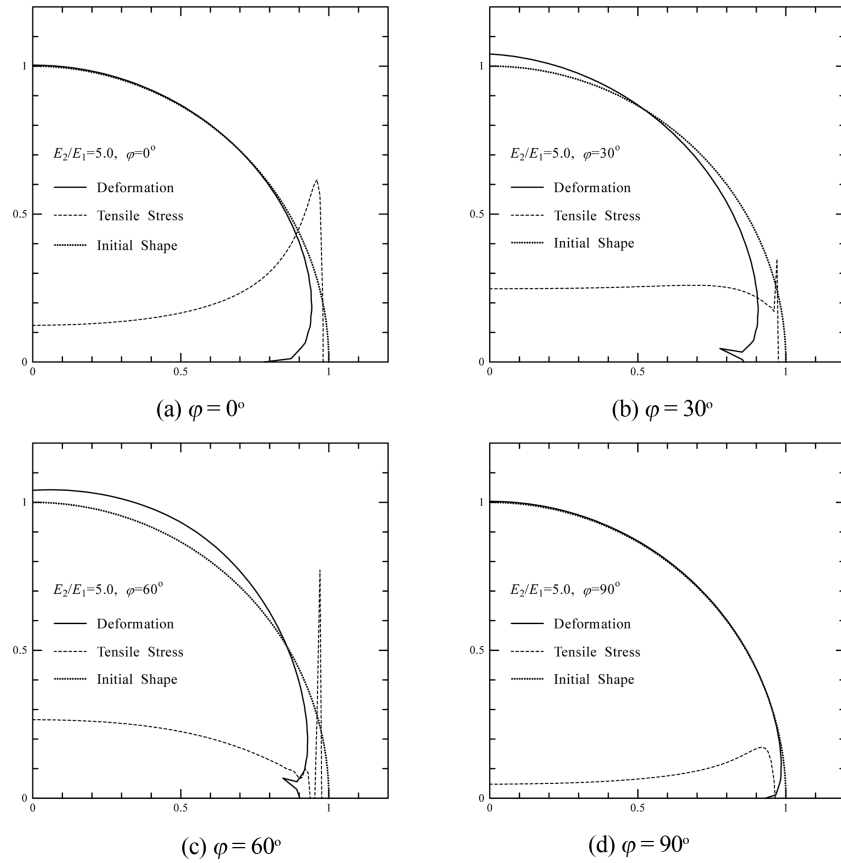
(d) $\varphi = 90°$

Fig. 13 Relation between distribution of tensile stress and deformation

maximum tensile stress occurs near the loading point. The tensile stress on the loading radius decreases as the distance from the loading point increases, and the minimum tensile stress occurs at the center of the specimen. For both cases, it seems that the effect of the deformation on stresses is largest near the loading point because the tensile stresses near the loading points occur due to deformation along the loading axis. The maximum tensile stress and the displacement at the loading point for $\varphi = 0°$ are larger than those for $\varphi = 90°$. For $\varphi = 30°$, the direction of deformation at the loading point does not correspond to the loading direction. Also, the maximum value and the minimum value do not appear clearly. For $\varphi = 60°$, the direction of the deformation at the loading point does not also correspond to the loading direction, and the angle between these directions is larger than that for $\varphi = 30°$. For both cases, it seems that stresses which occurred at the center are lager than those for $\varphi = 0°$ and $90°$ because the deformation does not correspond to the loading direction.

5. Conclusions

For the diametrical compression tests of orthotropic materials, an analysis with a theoretical

solution has been presented by Chen *et al.* (1998), Exadaktylos and Kaklis (2001), Exadaktylos (2001) and Claesson and Bohloli (2002), and another analysis based on the finite element method has been presented by Lemmon and Blackketter (1996). However, these analyses are made under the plane stress condition and their application is limited to tests on thin specimens.

In this paper, the authors made up an equation lacking in Lekhnitskii's theoretical solution and presented a model of the problem under the plane strain condition. This permitted a numerical analysis not only of tensile stress but also of the displacement obtained under diametrical compression tests for column-shaped specimens of orthotropic materials. In addition, the concentrated stress, which could not be represented by the finite element method, can now be successfully represented.

From the present numerical results, it can be observed that the distribution of tensile stress on the loading radius depends on the angle between the loading direction and the principal elastic axis, as in the case of the plane stress condition. In addition, it has been found that the tensile stress under the plane stress condition and that under the plane strain condition are different, and that the difference increases with increasing the orthotropy ratio. Furthermore, the deformation of the surface and the displacements on the loading radius are calculated and compared with the corresponding values under the plane stress condition in graphical form. Finally, the relation between the deformation and the distribution of tensile stress on the loading radius are shown in graphical form.

References

Cai, M. and Kaiser, P.K. (2004), "Numerical simulation of the Brazilian test and the tensile strength of anisotropic rocks and rocks with pre-existing cracks", *Int. J. Rock Mech. Min.*, **41**, 450-451.

Cauweleart, F.V. and Eckmann, B. (1994), "Indirect tensile test applied to anisotropic materials", *Mater. Struct.*, **27**, 54-60.

Chen, C.S., Pan, E. and Amadei, B. (1998), "Determination of deformability and tensile strength of anisotropic rock using brazilian tests", *Int. J. Rock Mech. Min.*, **35**, 43-61.

Claesson, J. and Bohloli, B. (2002), "Brazilian test: stress field and tensile strength of anisotropic rocks using an analytical solution", *Int. J. Rock Mech. Min.*, **39**, 991-1004.

Exadaktylos, G.E. and Kaklis, K.N. (2001), "Applications of an explicit solution for the transversely isotropic circular disc compressed diametrically", *Int. J. Rock Mech. Min.*, **38**, 227-243.

Exadaktylos, G.E. (2001), "On the constraints and relations of elastic constants of transversely isotropic geomaterials", *Int. J. Rock Mech. Min.*, **38**, 941-956.

Jianhon, Y., Wu, F.Q. and Sun, J.Z. (2009), "Estimation of the tensile elastic modulus using Brazilian disc by applying diametrically opposed concentrated loads", *Int. J. Rock Mech. Min.*, **46**, 568-576.

Kawakubo, S., Tsutsumi, T. and Hirashima, K. (1996), "Stress and displacement fields for an anisotropic elliptical disk subjected to arbitrary loads at boundary", *Trans. JSME Series A,* **62**, 1626-1633. (in Japanese)

Lavrov, A. and Vervoort, A. (2002), "Theoretical treatment of tangential loading effects on the Brazilian test stress distribution", *Int. J. Rock Mech. Min.*, **39**, 275-283.

Lekhnitskii, S.G. (1968), *Anisotropic Plate*, Gordon & Breach, New York.

Lemmon, R.K. and Blackketter, D.M. (1996), "Stress analysis of an orthotropic material under diametral compression", *Exp. Mech.,* **36**, 204-211.

Markides, C.F., Pazis, D.N. and Kourkoulis, S.K. (2010), "Closed full-field solution for stresses and displacements in Brazilian disk under distributed radial load", *Int. J. Rock Mech. Min.*, **47**, 227-237.

Sokolnikoff, I.S. (1956), *Mathematical Theory of Elasticity*, McGraw-Hill, New York.

Tavallali, A. and Vervoort, A. (2010), "Effect of layer orientation on the failure of layered sandstone under

Brazilian test conditions", *Int. J. Rock Mech. Min.*, **47**, 313-322.

Timoshenko, S.P and Goodier, J.N. (1970), *Theory of Elasticity*, McGraw-Hill, New York.

Tsutsumi, T. and Hirashima, K. (2000), "Analysis of orthotropic circular disks and rings under diametrical loading", *Struct. Eng. Mech.*, **9**(1), 37-50.